1-1-2003

Finite Element Solutions of Heat Transfer in Molten Polymer Flow in Tubes with Viscous Dissipation

Dongming Wei
University of New Orleans, dwei@uno.edu

Haibiao Luo

Available online at www.sciencedirect.com
SCIENCE DIRECT®
PERGAMON
International Journal of Heat and Mass Transfer 46 (2003) 3097–3108
International Journal of HEAT and MASS TRANSFER
www.elsevier.com/locate/ijhmt

Finite element solutions of heat transfer in molten polymer flow in tubes with viscous dissipation

Dongming Wei *, Haibiao Luo

Department of Mathematics, University of New Orleans, New Orleans, LA 70148, USA

Received 1 April 2002; received in revised form 13 November 2002

Abstract

This paper presents the results of finite element analysis of a heat transfer problem of flowing polymer melts in a tube with constant ambient temperature. The rheological behavior of the melt is described by a temperature dependent power-law model. A viscous dissipation term is included in the energy equation. Temperature profiles are obtained for different tube lengths and different entrance temperatures. The results are compared with some similar results in the literature.

Keywords: Heat transfer; Finite element solutions; Tubes; Power-law flows; Polymer flows; Viscous dissipation; Graetz–Nusselt problem

1. Introduction

Heat transfer to incompressible viscous non-Newtonian fluids is a problem of considerable practical significance since many fluids in food processing, polymer processing, and biochemical industries undergo a heat exchange process either during their preparation or in their application.

The so-called Graetz–Nusselt problem which has been studied for nearly 100 years for heat transfer of Newtonian flows in tubes is to solve for temperature profiles in the fluid flows in circular tubes. The following assumptions are frequently made in solving the Graetz–Nusselt problem as summarized in [11]:

(1) temperature has reached a steady state;
(2) heat conduction in the tube direction is negligible in comparison with heat transport in the tube direction by the over all fluid motion;
(3) the equilibrium physical property ρ (density) and C_p (heat capacity) are independent of position;
(4) the non-equilibrium property η (viscosity) is independent of position, and k (thermal conductivity) is independent of position;
(5) heat produced by viscous dissipation is negligible;
(6) there are no external (body) forces acting on the fluid;
(7) the flow obeys Newton's law of viscosity and Fourier's law of heat conduction.

Lyche and Bird [11] considered the problem for power-law flows with no viscous dissipation. Their work is concerned with the relaxation of the seventh assumption and seems to be the first to find an analytic solution of the Graetz–Nusselt problem for a non-Newtonian flow. The power-law fluid has been proven useful for the description of polymer melts, metal melts, blood flow as well as many other industrial flows [6]. In this paper, we study the Graetz–Nusselt problem with the following assumptions:

(1) η is a function of position and temperature;
(2) heat conduction in the tube direction is not negligible;
(3) heat produced by viscous dissipation is not negligible and it satisfies an Arrhenius temperature dependence law;

* Corresponding author.

0017-9310/03/$ - see front matter
doi:10.1016/S0017-9310(03)00069-3

Nomenclature

A^e	the triangle cross section of Ω^e
$\|A^e\|$	area of triangle A^e
A, B	constant coefficients in Eq. (2.3)
b	shear rate viscosity
B_r	Brinkman number
C, D	constant coefficients in Eq. (2.8)
C_p	specific heat capacity
$\mathbf{F}$, $\mathbf{F}^e$	global and local load vectors
h	convective heat transfer coefficient
J	the Jocobian matrix
k	fluid thermal conductivity
$\mathbf{K}$, $\mathbf{K}^e$	global and local stiffness matrices
n	constant index in the power-law model
$\{\mathbf{N}\}$	linear shape function vector
r, R	dimensional, and non-dimensional radial coordinates
$\{\mathbf{R}\}$, $\{\mathbf{R}^e\}$	global and local residual vector in Eq. (3.1)
r_0	radius of the tube
S	surface area
T	dimensional temperature
T_{bulk}	bulk temperature
T_m	constant coefficient in Eq. (2.3)
T_0	inlet fluid temperature
T_w	tube wall temperature
T_∞	ambient temperature
u	flow velocity in the tube
u_{av}	mean flow velocity in the tube
z, Z	dimensional, and non-dimensional axial coordinates

Greek symbols

$\{\mathbf{\Phi}\}$	nodal temperature for a triangle finite element
Γ	arc length
Γ^e	boundary of A^e
η	apparent viscosity
v	constant coefficient in Eq. (2.5)
ρ	fluid density
τ	shear stress
Ω	solution domain
Ω^e	a general finite element subdomain numbered e

Superscripts and subscripts

T	transpose of a matrix
e	refers to a quantity or entity associated with Ω^e

(4) the flow obeys the Ostwald–deWaele law which is also called the power-law and Fourier's law of heat conduction.

The corresponding model is a non-linear elliptic boundary value problem. A general analytic solution of the model for the temperature profile in the tube is not available. Numerical methods are required to provide solutions to the problem, although Wei and Zhang [17] have shown an analytic temperature profile at large tube length. Several papers for this power-law flow Graetz-type problem can be found which use analytic or numerical approaches. For example, Shih et al. [16] investigated the entrance laminar heat transfer of power-law polymer fluids in circular tubes with wall slip by Leveque series which uses a linear velocity profile. Flores et al. [4] surveyed the heat transfer to power-law flow in tubes and flat ducts with viscous heat generation by superposition procedures. Kumar and Bhattacharya [7] studied the aseptic processing of incompressible non-Newtonian liquid food flow with temperature-dependent and shear viscosity. Due to the jump in the fluid inlet temperature and the tube wall temperature, the solution of the Graetz-type problems suffer a unbounded temperature gradient at the edge of the entrance. Prusa and Manglik [13] presented a singular perturbation based finite difference method for the solution of the power-law Graetz-type problem. Their method give high level of accuracy as the singularity is approached.

Most of these earlier research work was concerned with the temperature-independent viscosity power-law model. Shih et al. and Flores et al. have considered the viscous dissipation term $B_r r^{n+1}$ after dimensionless reduction, where B_r is called the Brinkman number, r is radial position, and n is the shear rate exponent. Kumar and Bhattacharya put temperature into consideration in their viscous dissipation term and used $\eta_\infty e^{N\Delta E/R_g T} r^{n-1}$, where η_∞, ΔE, R_g and n are constant coefficients. However, they only considered it in the equations of motion and neglected it in the equation of energy. In the present paper a temperature and position-dependent viscous dissipation term $A e^{-nB(T-T_m)}|du/dr|^{n-1}$ is considered, and heat conduction in the tube direction is included. This model came from Agur and Vlachopoulos's paper [1]. In their paper a typical high-density polyethylene melt was investigated, and numerical solutions were obtained by using a finite difference method. In all the above mentioned papers, heat conduction in the tube direction was neglected. The ambient temperature was applied directly to the fluid as a Dirichlet boundary condition, and the entrance temperature was used as the initial condition for the corresponding parabolic partial differential equation. Whereas, we include the conduction term in the tube

direction and solve a corresponding elliptic equation by using a Galerkin finite element method. We also allow convection through the ambient and obtain the corresponding solution with a Dirichlet boundary condition on the wall by letting the film coefficient approach infinity as a limit. There are several related papers (see, e.g., [2,3,9,10]) in which the following stress τ and shear rate $\mathrm{d}u/\mathrm{d}r$ relationship is adopted

$$\tau = \mu \frac{\dfrac{\mathrm{d}u}{\mathrm{d}r}}{\left(1 + \dfrac{\mu}{\mu_0}\left|\dfrac{\mathrm{d}u}{\mathrm{d}r}\right|^{1-n}\right)}$$

in order to compensate the loss of accuracy of the power-law

$$\tau = \mu \left|\frac{\mathrm{d}u}{\mathrm{d}r}\right|^{n-1} \frac{\mathrm{d}u}{\mathrm{d}r}$$

for some fluids in which effective viscosity does not vanish near the centerline of the tube. There are three powerful numerical methods which can be employed to solve this problem: finite differences, control volumes and finite elements. Since the finite element method has the ability to handle irregular geometrical boundaries and complex boundary conditions and can be easily modified to solve more general problems, it is our choice of numerical method to solve this problem. In the second section of the paper, we present the formulation of the boundary value problem to be used as our model of the tube problem. In the third section, we present the finite element formulation and an algorithm for computing the finite element solutions of the proposed model. Although the procedures described in this section are standard, we feel that it is necessary to explain some of the specific details for this particular application.

In the last section, we present numerical solutions obtained by running the finite element code which we develop based on the finite element algorithm. Analytical solutions of a Graetz–Nusselt problem provided by Flores et al. [4], which is a special case of our problem, are used to compare with the numerical solutions. The analytic solution at large tube length obtained by Wei and Zhang [17] is also used to validate our numerical solutions.

2. The mathematical model

We consider steady state heat transfer to hydrodynamically developed laminar flow of a non-Newtonian Poiseuille flow inside a circular tube subject to prescribed ambient temperature. The tube wall is smooth and no vibrations are present. The viscous dissipation in the fluid is assumed to be a function of radial position

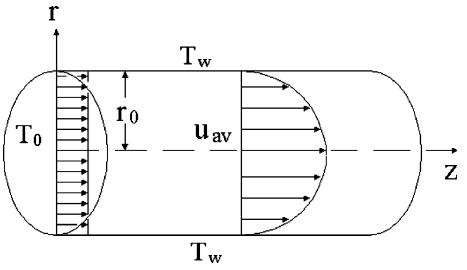

Fig. 1. Polymer flow in the tube.

and fluid temperature. We also consider free convection effects on the wall, and assume constant physical properties. Since the velocity profile is fully developed, the corresponding energy and velocity problems are decoupled. The mathematical model for this heat transfer problem is given by

$$\rho C_p u \frac{\partial T}{\partial z} = k\left(\frac{\partial^2 T}{\partial r^2} + \frac{1}{r}\frac{\partial T}{\partial r} + \frac{\partial^2 T}{\partial z^2}\right) + \tau \frac{\mathrm{d}u}{\mathrm{d}r} \tag{2.1}$$

where $T = T(r,z)$ is the unknown temperature of the flow at location (r,z) with $0 \leqslant r \leqslant r_0$, $0 \leqslant z < \infty$, and u is the velocity of the flow at the same location.

A common constitutive equation for polymer melts with viscous dissipation is (Fig. 1)

$$\tau = \eta \frac{\mathrm{d}u}{\mathrm{d}r} \tag{2.2}$$

where

$$\eta = A\,\mathrm{e}^{-nB(T-T_\mathrm{m})}\left|\frac{\mathrm{d}u}{\mathrm{d}r}\right|^{n-1} \tag{2.3}$$

By substituting (2.2) and (2.3) into the energy equation (2.1), we obtain

$$\rho C_p u \frac{\partial T}{\partial z} = k\left(\frac{\partial^2 T}{\partial r^2} + \frac{1}{r}\frac{\partial T}{\partial r} + \frac{\partial^2 T}{\partial z^2}\right) + \eta\left(\frac{\mathrm{d}u}{\mathrm{d}r}\right)^2 \tag{2.4}$$

In the above, ρ, C_p, k, A, B, T_m, and n are positive constants, and u is given by

$$u = u_\mathrm{av}\left(\frac{v+2}{v}\right)\left[1 - \left(\frac{r}{r_0}\right)^v\right] \tag{2.5}$$

in which r_0 is the radius of the tube, u_av is the mean flow velocity, and $v = (n+1)/n$. The constant n is called the power-law index which satisfies $0 < n < \infty$. The flows are frequently referred to as power-law flows. The constants are being obtained experimentally. The fully developed velocity profile is assumed due to a small Reynolds number given by $\rho U^{1-n}L^n/A$ in our example of application. Here the origin of the xy-plane is at the center of the cross-section of the tube at $z = 0$, the z-axis is in the tube flow direction and is placed through the

center of the tube. The boundary conditions for (2.4) are given by

$$\begin{cases} T(r,0) & = T_0 \\ T(r_0,z) & = T_w \\ \dfrac{\partial T(0,z)}{\partial r} & = 0 \\ \dfrac{\partial T(r,z)}{\partial z} & = 0 \quad \text{as } z \to \infty \end{cases} \tag{2.6}$$

where T_w is the tube wall temperature and T_0 the inlet fluid temperature. To be more general, in our finite element code, the Dirichlet boundary condition

$$T(r_0,z) = T_w$$

is approximated by the following mixed convective boundary condition

$$-k\frac{\partial T(r,z)}{\partial r} = h(T(r,z) - T_\infty) \tag{2.7}$$

where T_∞ is the ambient temperature in the exterior of the tube, h is the film coefficient. The condition $T(r_0,z) = T_w$ is satisfied approximately as h is chosen to be very large and the value of T_∞ is used to replace T_w.

All T_0, T_w, and T_∞ are constants in the work. Conditions upstream are assumed to maintain a uniform temperature T_0 for the entering fluid. The last condition in (2.6) will be replaced by

$$\frac{\partial T(r,z)}{\partial z} = 0$$

for a very large value z which is to be determined by the numerical temperature profiles obtained.

Introducing the dimensionless parameters

$$Z = \frac{vkz}{(v+2)\rho C_p u_{av} r_0^2}, \quad R = \frac{r}{r_0}$$

we have

$$\frac{\partial T}{\partial z} = \frac{vk}{(v+2)\rho C_p u_{av} r_0^2}\frac{\partial T}{\partial Z}$$

$$\frac{\partial^2 T}{\partial z^2} = \left(\frac{vk}{(v+2)\rho C_p u_{av} r_0^2}\right)^2 \frac{\partial^2 T}{\partial Z^2}$$

$$\frac{\partial T}{\partial r} = \frac{1}{r_0}\frac{\partial T}{\partial R}\frac{\partial^2 T}{\partial r^2} = \frac{1}{r_0^2}\frac{\partial^2 T}{\partial R^2}$$

$$\frac{du}{dr} = -u_{av}\frac{v+2}{r_0}R^{v-1}$$

and

$$\eta = \left[A\,e^{nBT_m}\left(u_{av}\frac{v+2}{r_0}\right)^{n-1}\right]R^{(v-1)(n-1)}\,e^{-nBT}$$

Since $v = (n+1)/n$, we get

$$\begin{aligned} \eta\left(\frac{du}{dr}\right)^2 &= \left[A\,e^{nBT_m}u_{av}\left(\frac{v+2}{r_0}\right)^{n-1}\right]R^{(v-1)(n-1)} \\ &\quad \times \left(u_{av}\frac{v+2}{r_0}R^{v-1}\right)^2 e^{-nBT} \\ &= \left[A\,e^{nBT_m}u_{av}^{n+1}\left(\frac{v+2}{r_0}\right)^{n+1}\right]R^{(v-1)(n+1)}\,e^{-nBT} \\ &= \left[A\,e^{nBT_m}u_{av}^{n+1}\left(\frac{v+2}{r_0}\right)^{n+1}\right]R^{v}\,e^{-nBT} \end{aligned}$$

From the above calculations and (2.4), we then have the following non-linear elliptic partial differential equation

$$(1-R^v)\frac{\partial T}{\partial Z} = D\frac{\partial^2 T}{\partial Z^2} + \frac{1}{R}\frac{\partial T}{\partial R} + \frac{\partial^2 T}{\partial R^2} + C\,e^{-BnT}R^v \tag{2.8}$$

where

$$D = \left(\frac{vk}{(v+2)\rho C_p u_{av} r_0}\right)^2$$

$$C = \frac{u_{av}^{n+1}}{k}A\,e^{BnT_m}\frac{(v+2)^{n+1}}{r_0^{n-1}}$$

and

$$\eta = \frac{Ck}{u_{av}^2(v+2)^2}R^{(v-1)(n-1)}\,e^{-nBT}$$

In the above, if the quantity D is very small and the corresponding term $D\partial^2 T/\partial Z^2$ in (2.8) being neglected, then the equation is changed from an elliptic type to a parabolic type which was considered in [1]. Eq. (2.8) and the boundary conditions (2.6) and (2.7) form a well-posed non-linear elliptic boundary value problem as discussed in [17], where it is shown that the solution of the elliptic problem converges to the solution of the parabolic problem as $D \to 0^+$.

The example which we shall use for numerical solutions is based on this formulation of the problem. The data used in the example was given in [1].

3. The finite element model

We shall use a Galerkin finite element method for numerical solutions of the problem defined by (2.7), (2.8), and $T(0,R) = T_0$. There are many introductory books which provide details about this method (see, e.g., [14,15]). In the Galerkin finite element procedure, the solution domain Ω is divided into subdomains Ω^e, which

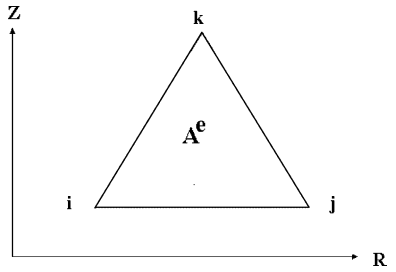

Fig. 2. The cross-section A^e of a axisymmetric linear triangular element Ω^e.

are called finite elements (see Fig. 2), and in each subdomain we seek the solution of the governing equation through a piecewise approximation to the solution. The differential equations must be recast into an approximate integral form which is the basis for the finite element formulation. Due to symmetry, we shall use axisymmetric finite elements. For simplicity, each subdomain is chosen to be a ring obtained by revolving about the Z-axis 360° a triangle in the (R,Z) plane. In the following such a subdomain is denoted by $\Omega^e = [0,2\pi)\times A^e$, where A^e denotes the associated triangle and the superscript e is used to count the number of subdomains involved. The three vertices of the triangle are labeled by i, j, and k or 1, 2, and 3 respectively. We also chose piecewise linear interpolation functions within each element. Let $\{\mathbf{N}\} = [N_1, N_2, N_3]^{\mathrm{T}}$ denote the three linear interpolation shape functions of (R,Z). We begin the Galerkin procedure by constructing the weak integral form of (2.8), and have

$$\{\mathbf{R}^e\} = \int_{\Omega^e} \{\mathbf{N}\}\left[-\frac{\partial^2 T}{\partial R^2} - \frac{1}{R}\frac{\partial T}{\partial R} - D\frac{\partial^2 T}{\partial Z^2} + (1-R^v)\frac{\partial T}{\partial Z} - C\,\mathrm{e}^{-BnT}R^v \right] \mathrm{d}V \tag{3.1}$$

which can be written as

$$\{\mathbf{R}^e\} = \int_{\Omega^e} \{\mathbf{N}\}\left[-\frac{1}{R}\frac{\partial}{\partial R}\left(R\frac{\partial T}{\partial R}\right) - D\frac{\partial^2 T}{\partial Z^2} + (1-R^v)\frac{\partial T}{\partial Z} - C\,\mathrm{e}^{-BnT}R^v \right] \mathrm{d}V \tag{3.2}$$

Since

$$\frac{\{\mathbf{N}\}}{R}\frac{\partial}{\partial R}\left(R\frac{\partial T}{\partial R}\right) = \frac{1}{R}\frac{\partial}{\partial R}\left(\{\mathbf{N}\}R\frac{\partial T}{\partial R}\right) - \frac{\partial\{\mathbf{N}\}}{\partial R}\frac{\partial T}{\partial R} \tag{3.3}$$

and

$$\{\mathbf{N}\}\frac{\partial^2 T}{\partial Z^2} = \frac{\partial}{\partial Z}\left(\{\mathbf{N}\}\frac{\partial T}{\partial Z}\right) - \frac{\partial\{\mathbf{N}\}}{\partial Z}\frac{\partial T}{\partial Z} \tag{3.4}$$

by substituting (3.3) and (3.4) into the weighted residual equation (3.2), we have

$$\begin{aligned}\{\mathbf{R}^e\} = {} & \int_{\Omega^e}\left[\frac{\partial\{\mathbf{N}\}}{\partial R}\frac{\partial T}{\partial R} + D\frac{\partial\{\mathbf{N}\}}{\partial Z}\frac{\partial T}{\partial Z}\right]\mathrm{d}V \\ & - \int_{\Omega^e}\left[\frac{1}{R}\frac{\partial}{\partial R}\left(\{\mathbf{N}\}R\frac{\partial T}{\partial R}\right) + D\frac{\partial}{\partial Z}\left(\{\mathbf{N}\}\frac{\partial T}{\partial Z}\right)\right]\mathrm{d}V + \int_{\Omega^e}\{\mathbf{N}\}(1-R^v)\times\frac{\partial T}{\partial Z}\mathrm{d}V - \int_{\Omega^e}\{\mathbf{N}\}C\,\mathrm{e}^{-BnT}R^v\,\mathrm{d}V\end{aligned} \tag{3.5}$$

Let

$$\{\mathbf{\Phi}\} = [\,T_i \quad T_j \quad T_k\,]^{\mathrm{T}} \tag{3.6}$$

and

$$T = \{\mathbf{N}\}^{\mathrm{T}}\{\mathbf{\Phi}\} \tag{3.7}$$

then

$$\frac{\partial T}{\partial R} = \frac{\partial\{\mathbf{N}\}^{\mathrm{T}}}{\partial R}\{\mathbf{\Phi}\} \tag{3.8}$$

$$\frac{\partial T}{\partial Z} = \frac{\partial\{\mathbf{N}\}^{\mathrm{T}}}{\partial Z}\{\mathbf{\Phi}\} \tag{3.9}$$

Substituting (3.6)–(3.9) into Eq. (3.5), we have

$$\begin{aligned}\{\mathbf{R}^e\} = {} & \int_{\Omega^e}\left[\frac{\partial\{\mathbf{N}\}}{\partial R}\frac{\partial\{\mathbf{N}\}^{\mathrm{T}}}{\partial R} + D\frac{\partial\{\mathbf{N}\}}{\partial Z}\frac{\partial\{\mathbf{N}\}^{\mathrm{T}}}{\partial Z}\right]\mathrm{d}V\{\mathbf{\Phi}\} \\ & - \int_{\Omega^e}\left[\frac{1}{R}\frac{\partial}{\partial R}\left(\{\mathbf{N}\}R\frac{\partial T}{\partial R}\right) + D\frac{\partial}{\partial Z}\left(\{\mathbf{N}\}\frac{\partial T}{\partial Z}\right)\right]\mathrm{d}V \\ & + \int_{\Omega^e}\{\mathbf{N}\}(1-R^v)\frac{\partial\{\mathbf{N}\}^{\mathrm{T}}}{\partial Z}\mathrm{d}V\{\mathbf{\Phi}\} - \int_{\Omega^e}\{\mathbf{N}\}C\,\mathrm{e}^{-BnT}R^v\,\mathrm{d}V\end{aligned} \tag{3.10}$$

The second volume integral in (3.10) can be reduced to a surface integral by using the Divergence Theorem, and we have

$$\begin{aligned}\{\mathbf{R}^e\} = {} & \int_{\Omega^e}\left[\frac{\partial\{\mathbf{N}\}}{\partial R}\frac{\partial\{\mathbf{N}\}^{\mathrm{T}}}{\partial R} + D\frac{\partial\{\mathbf{N}\}}{\partial Z}\frac{\partial\{\mathbf{N}\}^{\mathrm{T}}}{\partial Z}\right]\mathrm{d}V\{\mathbf{\Phi}\} - \int_{\partial\Omega^e}\left[\{\mathbf{N}\}\frac{\partial T}{\partial R}\cos\theta + D\frac{\partial T}{\partial Z}\sin\theta\right]\mathrm{d}S + \int_{\Omega^e}\{\mathbf{N}\}(1-R^v)\frac{\partial\{\mathbf{N}\}^{\mathrm{T}}}{\partial Z}\mathrm{d}V\{\mathbf{\Phi}\} \\ & - \int_{\Omega^e}\{\mathbf{N}\}C\,\mathrm{e}^{-BnT}R^v\,\mathrm{d}V\end{aligned} \tag{3.11}$$

where $\partial\Omega^e = [0,2\pi)\times\Gamma^e$ is used to denote the boundary of Ω^e. The derivative boundary condition is given by normal flux

$$\{\mathbf{I}^e\} = -\int_{\partial\Omega^e}\{\mathbf{N}\}\left(\frac{\partial T}{\partial R}\cos\theta + D\frac{\partial T}{\partial Z}\sin\theta\right)\mathrm{d}S$$
$$= -2\pi\int_{\Gamma^e}\{\mathbf{N}\}h(T_\infty - T)\,\mathrm{d}\Gamma$$
$$= 2\pi\int_{\Gamma^e}\{\mathbf{N}\}hT\,\mathrm{d}\gamma - 2\pi\int_{\Gamma^e}\{\mathbf{N}\}hT_\infty\,\mathrm{d}\Gamma$$

Substituting (3.7) into the above equation, we have

$$\{\mathbf{I}^e\} = 2\pi\int_{\Gamma^e}[\{\mathbf{N}\}h\{\mathbf{N}\}^\tau\{\mathbf{\Phi}\} - \{\mathbf{N}\}hT_\infty]\,\mathrm{d}\Gamma \tag{3.12}$$

Let

$$[\mathbf{K}_k^e] = \int_{\Omega^e}\left[\frac{\partial\{\mathbf{N}\}}{\partial R}\frac{\partial\{\mathbf{N}\}^\mathrm{T}}{\partial R} + D\frac{\partial\{\mathbf{N}\}}{\partial Z}\frac{\partial\{\mathbf{N}\}^\mathrm{T}}{\partial Z}\right]\mathrm{d}V \tag{3.13}$$

$$[\mathbf{K}_s^e] = 2\pi\int_{\Gamma^e}\{\mathbf{N}\}h\{\mathbf{N}\}^\tau\,\mathrm{d}\Gamma \tag{3.14}$$

$$\{\mathbf{F}_s^e\} = 2\pi\int_{\Gamma^e}\{\mathbf{N}\}hT_\infty\,\mathrm{d}\Gamma \tag{3.15}$$

Then

$$\{\mathbf{I}^e\} = [\mathbf{K}_s^e]\{\mathbf{\Phi}\} - \{\mathbf{F}_s^e\} \tag{3.16}$$

The shape functions for the linear axisymmetric triangular element are

$$N_i = \frac{1}{2|A^e|}(a_i + b_iR + c_iZ) \tag{3.17}$$

$$N_j = \frac{1}{2|A^e|}(a_j + b_jR + c_jZ) \tag{3.18}$$

$$N_k = \frac{1}{2|A^e|}(a_k + b_kR + c_kZ) \tag{3.19}$$

where

$$a_i = R_jZ_k - R_kZ_j,\quad a_j = R_kZ_i - R_iZ_k,\quad a_k = R_iZ_j - R_jZ_i$$
$$b_i = Z_j - Z_k,\quad b_j = Z_k - Z_i,\quad b_k = Z_i - Z_j$$
$$c_i = R_j - R_k,\quad c_j = R_k - R_i,\quad c_k = R_i - R_j$$

where (R_i, Z_i), (R_j, Z_j), and (R_k, Z_k) denote the coordinates of the three vertices and $|A^e|$ the area of the triangle A^e. Let

$$L_1 = N_i,\quad L_2 = N_j,\quad L_3 = N_k$$

Then the area integral is

$$\int_{A^e}L_1^\alpha L_2^\beta L_3^\gamma\,\mathrm{d}A = \frac{\alpha!\beta!\gamma!}{(\alpha+\beta+\gamma+2)!}2|A^e| \tag{3.20}$$

where α, β, γ are non-negative integers. By using the area integral equation and substituting (3.17)–(3.19) into (3.13), the evaluation of the stiffness element matrices (3.13) is

$$[\mathbf{K}_k^e] = \frac{2\pi R_{\mathrm{av}}k}{4|A^e|}\left\{\begin{bmatrix} b_i^2 & b_ib_j & b_ib_k \\ b_ib_j & b_j^2 & b_jb_k \\ b_ib_k & b_jb_k & b_k^2 \end{bmatrix} + \begin{bmatrix} c_i^2 & c_ic_j & c_ic_k \\ c_ic_j & c_j^2 & c_jc_k \\ c_ic_k & c_jc_k & c_k^2 \end{bmatrix}\right\} \tag{3.21}$$

where

$$R_{\mathrm{av}} = \frac{R_i + R_j + R_k}{3}$$

Substituting (3.17)–(3.19) into (3.14), we have

$$[\mathbf{K}_s^e] = 2\pi\int_{\Gamma^e}\{\mathbf{N}\}h\{\mathbf{N}\}^\tau\,\mathrm{d}\Gamma$$
$$= \frac{2\pi hL_{ij}}{12}\begin{bmatrix} 3R_i + R_j & R_i + R_j & 0 \\ R_i + R_j & R_i + 3R_j & 0 \\ 0 & 0 & 0 \end{bmatrix}$$

or

$$\frac{2\pi hL_{jk}}{12}\begin{bmatrix} 3R_i + R_k & 0 & R_i + R_k \\ 0 & 0 & 0 \\ R_i + R_k & 0 & R_i + 3R_k \end{bmatrix}$$

or

$$\frac{2\pi hL_{ik}}{12}\begin{bmatrix} 0 & 0 & 0 \\ 0 & 3R_j + R_k & R_j + R_k \\ 0 & R_j + R_k & R_j + 3R_k \end{bmatrix}$$

Similarly, we have

$$\{\mathbf{F}_s^e\} = \frac{2\pi hT_\infty L_{ij}}{6}\begin{Bmatrix} 2R_i + R_j \\ R_i + 2R_j \\ 0 \end{Bmatrix}$$

or

$$\frac{2\pi hT_\infty L_{jk}}{6}\begin{Bmatrix} 0 \\ 2R_j + R_k \\ R_j + 2R_k \end{Bmatrix}$$

or

$$\frac{2\pi hT_\infty L_{ik}}{6}\begin{Bmatrix} 2R_i + R_k \\ 0 \\ R_i + 2R_k \end{Bmatrix}$$

where $L_{i,j}$ denotes the length of the side of triangle A^e connecting vertex i and vertex j. Let

$$[\mathbf{K}_u^e] = \int_{\Omega^e}\{\mathbf{N}\}(1 - R^v)\frac{\partial\{\mathbf{N}\}^\mathrm{T}}{\partial Z}\mathrm{d}V \tag{3.22}$$

and

$$\{\mathbf{Q}^e\} = \int_{\Omega^e}\{\mathbf{N}\}C\,\mathrm{e}^{-BnT^e}R^v\,\mathrm{d}V \tag{3.23}$$

$[\mathbf{K}_u^e]$, $\{\mathbf{Q}^e\}$ and $\nabla\{\mathbf{Q}^e\}$ are evaluated by the Gauss–Legendre integration method in the triangular region. Since the lowest order of L_1, L_2 and L_3 in the integrand of $[\mathbf{K}_u^e]$, $\{\mathbf{Q}^e\}$ and $\nabla\{\mathbf{Q}^e\}$ is $2+v+1=4+1/n$, we choose a 4th order Gauss integration scheme which uses seven Gauss points for evaluations of these terms. We will use the following Gauss–Legendre integration formula for evaluations of the finite element matrices:

$$\int_{A^e} f(R,Z)\,\mathrm{d}R\,\mathrm{d}Z = \int_0^1 \int_0^{1-L_2} g(L_1,L_2,L_3)|J|\,\mathrm{d}L_1\,\mathrm{d}L_2 = \frac{1}{2}\sum_{l=1}^{7} w_l g_l |J|$$

where

$$|J| = \begin{vmatrix} \dfrac{\partial R}{\partial L_1} & \dfrac{\partial Z}{\partial L_1} \\ \dfrac{\partial R}{\partial L_2} & \dfrac{\partial Z}{\partial L_2} \end{vmatrix} = \begin{vmatrix} R_1-R_3 & Z_2-Z_3 \\ R_2-R_3 & Z_2-Z_3 \end{vmatrix}$$

is the Jacobian and the subscript l is used to denote evaluation of a function at the lth Gauss point. See, e.g., [14] or [15] for values of the Gaussian weights w_l and Gaussian points. Let $R=L_1R_1+L_2R_2+L_3R_3$, $Z=L_1Z_1+L_2Z_2+L_3Z_3$, and $T=T_1N_1+T_2N_2+T_3N_3$. We have

$$\begin{aligned}
[\mathbf{K}_u^e] &= \int_{\Omega^e} \{\mathbf{N}\}(1-R^v)\frac{\partial\{\mathbf{N}\}^{\mathrm{T}}}{\partial Z}\,\mathrm{d}V \\
&= 2\pi\int_{A^e} \{\mathbf{N}\}(1-R^v)\frac{\partial\{\mathbf{N}\}^{\mathrm{T}}}{\partial Z} R\,\mathrm{d}R\,\mathrm{d}Z \\
&= 2\pi\int_{A^e} \begin{Bmatrix} N_1 \\ N_2 \\ N_3 \end{Bmatrix} \begin{Bmatrix} \dfrac{\partial N_1}{\partial Z} & \dfrac{\partial N_2}{\partial Z} & \dfrac{\partial N_3}{\partial Z} \end{Bmatrix} \times (1-R^v)R\,\mathrm{d}R\,\mathrm{d}Z \\
&= 2\pi\int_{A^e} \begin{bmatrix} N_1\dfrac{\partial N_1}{\partial Z} & N_1\dfrac{\partial N_2}{\partial Z} & N_1\dfrac{\partial N_3}{\partial Z} \\ N_2\dfrac{\partial N_1}{\partial Z} & N_2\dfrac{\partial N_2}{\partial Z} & N_2\dfrac{\partial N_3}{\partial Z} \\ N_3\dfrac{\partial N_1}{\partial Z} & N_3\dfrac{\partial N_2}{\partial Z} & N_3\dfrac{\partial N_3}{\partial Z} \end{bmatrix} \times (1-R^v)R\,\mathrm{d}R\,\mathrm{d}Z \\
&= \pi\sum_{l=1}^{7} w_l \begin{bmatrix} L_1\dfrac{\partial L_1}{\partial Z} & L_1\dfrac{\partial L_2}{\partial Z} & L_1\dfrac{\partial L_3}{\partial Z} \\ L_2\dfrac{\partial L_1}{\partial Z} & L_2\dfrac{\partial L_2}{\partial Z} & L_2\dfrac{\partial L_3}{\partial Z} \\ L_3\dfrac{\partial L_1}{\partial Z} & L_3\dfrac{\partial L_2}{\partial Z} & L_3\dfrac{\partial L_3}{\partial Z} \end{bmatrix}_l \{1-R_l^v\}R_l|J|
\end{aligned}$$

and

$$\begin{aligned}
\{\mathbf{Q}^e\} &= C\int_{\Omega^e} \{\mathbf{N}\}\mathrm{e}^{-BnT}R^v\,\mathrm{d}V \\
&= 2\pi C\int_{A^e} \{\mathbf{N}\}\mathrm{e}^{-BnT}R^{v+1}\,\mathrm{d}R\,\mathrm{d}Z \\
&= 2\pi C\int_0^1\int_0^{1-L_2} \begin{Bmatrix} L_1 \\ L_2 \\ L_3 \end{Bmatrix} \mathrm{e}^{-BnT}R^{v+1}|J|\,\mathrm{d}L_1\,\mathrm{d}L_2 \\
&= \pi C|J|\sum_{l=1}^{7} w_l \begin{Bmatrix} L_1 \\ L_2 \\ L_3 \end{Bmatrix}_l \mathrm{e}^{-BnT_l}R_l^{v+1}
\end{aligned}$$

The gradient of $\mathbf{Q}^e$ with respect to $\{\mathbf{\Phi}\}$ is given by

$$\nabla\{\mathbf{Q}^e\} = \begin{bmatrix} \dfrac{\partial Q_1^e}{\partial T_1} & \dfrac{\partial Q_1^e}{\partial T_2} & \dfrac{\partial Q_1^e}{\partial T_3} \\ \dfrac{\partial Q_2^e}{\partial T_1} & \dfrac{\partial Q_2^e}{\partial T_2} & \dfrac{\partial Q_2^e}{\partial T_3} \\ \dfrac{\partial Q_3^e}{\partial T_1} & \dfrac{\partial Q_3^e}{\partial T_2} & \dfrac{\partial Q_3^e}{\partial T_3} \end{bmatrix}$$

which is needed in order to implement Newton's iterations. Evaluation of the entry $\partial Q_i^e/\partial T_j$ in the above matrix $\nabla\{\mathbf{Q}^e\}$ is given by

$$\begin{aligned}
\frac{\partial Q_i^e}{\partial T_j} &= \frac{\partial}{\partial T_j}\left(2\pi C\int_{A^e} N_i\mathrm{e}^{-BnT}R^{v+1}\,\mathrm{d}R\,\mathrm{d}Z\right) \\
&= -2\pi CBn\int_{A^e} N_iN_j\mathrm{e}^{-BnT}R^{v+1}\,\mathrm{d}R\,\mathrm{d}Z \\
&= -2\pi CBn\int_0^1\int_0^{1-L_2} L_iL_j\mathrm{e}^{-BnT}R^{v+1}|J|\,\mathrm{d}L_1\,\mathrm{d}L_2 \\
&= -\pi CBn|J|\sum_{l=1}^{7} w_l(L_i)_l(L_j)_l\mathrm{e}^{-BnT_l}R_l^{v+1}
\end{aligned}$$

Similarly, we have the evaluation of the matrix $\nabla\{\mathbf{Q}^e\}$,

$$\nabla\{\mathbf{Q}^e\} = -\pi CBn|J|\sum_{l=1}^{7} w_l\mathrm{e}^{-BnT_l}R_l^{v+1}\begin{bmatrix} L_1^2 & L_1L_2 & L_1L_3 \\ L_2L_1 & L_2^2 & L_2L_3 \\ L_3L_1 & L_3L_2 & L_3^2 \end{bmatrix}_l$$

In the above Gauss integration formulas, $T_l=T_1(L_1)_l+T_2(L_2)_l+T_3(L_3)_l$, and $R_l=(L_1)_lR_1+(L_2)_lR_2+(L_3)_lR_3$, $1\leqslant l\leqslant 7$.

The solution domain Ω is divided into over 2000 triangular elements Ω^e for numerical simulation. Fig. 3 shows only 100 of these elements. Since this energy equation is non-linear, Newton's iteration method, which will give quadratic convergence to the solution, is used to solve the equation. The standard Gauss–Jordon elimination and the backward substitution method is used to solve the linear algebraic equation at each iteration. The solution of the linear energy equation is used as the initial solution to start Newton's iterations.

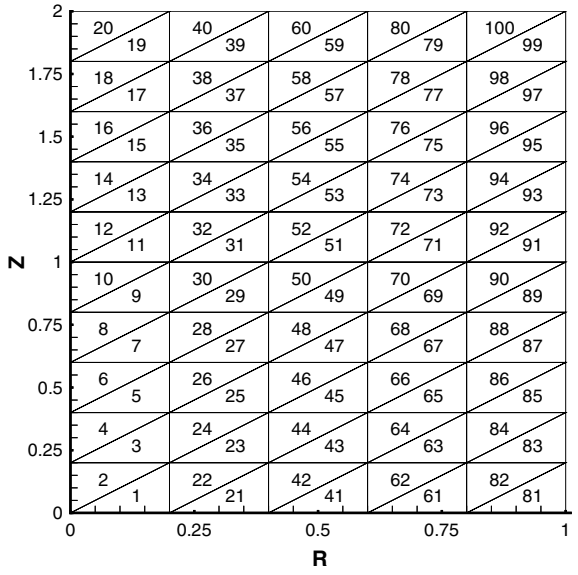

Fig. 3. The finite element mesh.

The linear energy equation without dissipation is given as the following

$$(1-R^v)\frac{\partial T}{\partial Z}=D\frac{\partial^2 T}{\partial Z^2}+\frac{1}{R}\frac{\partial T}{\partial R}+\frac{\partial^2 T}{\partial R^2} \tag{3.24}$$

It's global finite element matrix equation can be written as

$$[\mathbf{K}]\{\mathbf{\Phi}\}=\{\mathbf{F}\} \tag{3.25}$$

where

$$[\mathbf{K}]=[\mathbf{K}_k]+[\mathbf{K}_u]+[\mathbf{K}_s]$$
$$\{\mathbf{F}\}=\{\mathbf{F}_s\}$$

After the solution of the above linear energy equation is found, it will be used as an initial solution to solve the following non-linear energy equation with a dissipation term

$$(1-R^v)\frac{\partial T}{\partial Z}=D\frac{\partial^2 T}{\partial Z^2}+\frac{1}{R}\frac{\partial T}{\partial R}+\frac{\partial^2 T}{\partial R^2}+C\,\mathrm{e}^{-BnT}R^v \tag{3.26}$$

It's global matrix equation can be written as

$$[\mathbf{K}]\{\mathbf{\Phi}\}=\{\mathbf{F}\}+\{\mathbf{Q}\} \tag{3.27}$$

Newton's iteration method for a non-linear system

$$\{\mathbf{\Phi}^{n+1}\}=\{\mathbf{\Phi}^n\}-J(\mathbf{\Phi}^n)^{-1}\{\mathbf{R}(\mathbf{\Phi}^n)\} \tag{3.28}$$

can be written in the following form to avoid evaluating the inverse of the Jacobian matrix

$$J(\mathbf{\Phi}^n)\{\mathbf{\Phi}^{n+1}\}=J(\mathbf{\Phi}^n)\{\mathbf{\Phi}^n\}-\{\mathbf{R}(\mathbf{\Phi}^n)\} \tag{3.29}$$

where the Jacobian matrix $J(\mathbf{\Phi}^n)$ is

$$J(\mathbf{\Phi}^n)=\nabla R(\mathbf{\Phi}^n)=[\mathbf{K}]\{\mathbf{\Phi}^n\}-\nabla\{\mathbf{Q}\}$$

The corresponding computational scheme is

Input: number N of equations and unknowns; initial solution $\mathbf{\Phi}_0$; tolerance TOL; maximum number of iteration M.
Output: approximate solution $\mathbf{\Phi}$ or a message that the maximum number of iteration was exceeded.
Step 1. Set $k=1$
Step 2. While $(k\leqslant M)$ do steps 3–6
Step 3. Calculate $R(\mathbf{\Phi})$ and $J(\mathbf{\Phi})$
Step 4. Solve the $N\times N$ linear system $J(\mathbf{\Phi})\mathbf{\Theta}=J(\mathbf{\Phi})\mathbf{\Phi}-F(\mathbf{\Phi})$ for $\mathbf{\Theta}$
Step 5. If $\|\mathbf{\Theta}-\mathbf{\Phi}\|<\mathrm{TOL}$, then output $\mathbf{\Theta}$; (procedure completed successfully)
Stop
Step 6. Set $k=k+1$, $\mathbf{\Phi}=\mathbf{\Theta}$
Step 7. Output (Maximum number of iterations exceeded); (procedure completed unsuccessfully)
Stop.

For a detail description of Newton's iterations see, e.g., [12].

4. Results and discussion

The following power-law temperature-dependent viscosity model with fluid properties representing a typical high-density polyethylene melt were used as our example of numerical simulation

$$\eta=A\,\mathrm{e}^{-nB(T-T_\mathrm{m})}\left|\frac{\mathrm{d}u}{\mathrm{d}r}\right|^{n-1}$$

where $A=28,200$ Pa s^n, $B=0.0240$ K^{-1} and $T_\mathrm{m}=399.5$ K. This is the example given by Agur and Vlachopoulos in [1]. The following velocity and temperature boundary conditions have been used

$$u=u_\mathrm{av}\left[\frac{v+2}{v}\right]\left[1-\left(\frac{r}{r_0}\right)^v\right]$$
$$T(r,0)=T_0$$
$$-k\frac{\partial T}{\partial r}(r_0,z)=h(T(r_0,z)-T_\infty)$$
$$\frac{\partial T}{\partial z}(r,L)=0$$

where $u_\mathrm{av}=15.0$ cm/s $v=(n+1)/n$, $n=0.453$, $r_0=0.125$ cm $T_0=130$ °C, $T_\infty=160$ °C, and a large value of 740 cm is used for L. The finite element code is written for convective boundary condition. It covers the Dirichlet boundary condition which places the ambient temperature directly to the fluid on the tube wall in the limiting case when h is given a very large artificial value as large as 10^6 W/m^2 K in our computation. This can be justified since

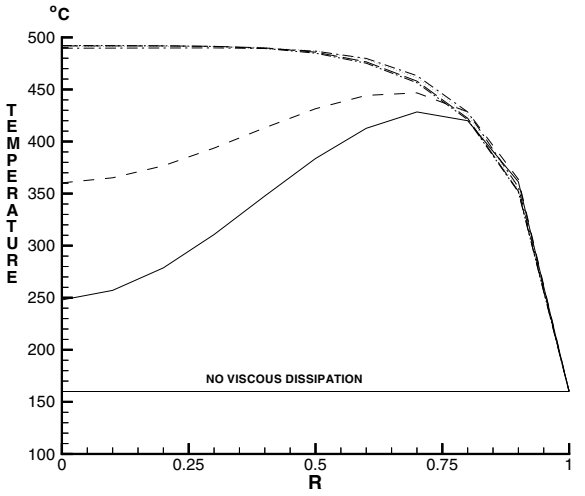

Fig. 4. Development of bulk temperature profiles along tube radial axis for the power-law flow at various tube lengths: $Z = 0.05$ (solid line), $Z = 0.1$ (dashed line), $Z = 0.5$ (dash dotted line), $Z = 1$ (dotted line), $Z = 1.5$ (long dashed line), $Z = 2.0$ (dash dot-dot line), and $Z = 2.5$ (solid line).

$$T(r_0,z) - T_\infty = -\frac{k}{h}\frac{\partial T}{\partial r}(r_0,z) = -10^{-6}k\frac{\partial T}{\partial r}(r_0,z)$$

can be very small and therefore $T(r_0,z)$ is close to T_∞. In this example, the value of D is 1.7667×10^{-7}, which is very small. Therefore the term $D\partial^2T/\partial Z^2$ is considered to be small and negligible by the authors of [1]. However, as one can see from the boundary conditions or the numerical solution presented in Fig. 6 that the quantity $\partial^2T/\partial Z^2$ can be very large at the entrance of the tube.

Solutions of the energy equation for Poiseuille flow through the tube with the above given data are presented in Figs. 4–6. The bulk temperature profiles in Figs. 4–6 are shown as functions of the dimensionless axial distance Z. The bulk temperature is defined as

$$T_{\text{bulk}}(Z) = \frac{\int_0^1 T(R,Z)u(R,Z)R\,\mathrm{d}R}{\int_0^1 u(R,Z)R\,\mathrm{d}R}$$

In Fig. 4, the temperature profiles for the power-law temperature-dependent viscosity model and for the model without viscosity are compared. The two models are identical except for the viscosity dissipation term which is zero in the second model. It can be seen that the temperature of the fluid obtained with the temperature-dependent model is much higher than the case without viscosity. And at the intermediate values of R, the temperature profiles bulge near the wall, indicating that more heat is generated by viscous dissipation here than is generated near the center of the tube. This is due to the fact that the shear rates are the highest near the tube walls. In Fig. 5, the bulk temperatures are shown for power-law temperature-dependent viscosity fluids with

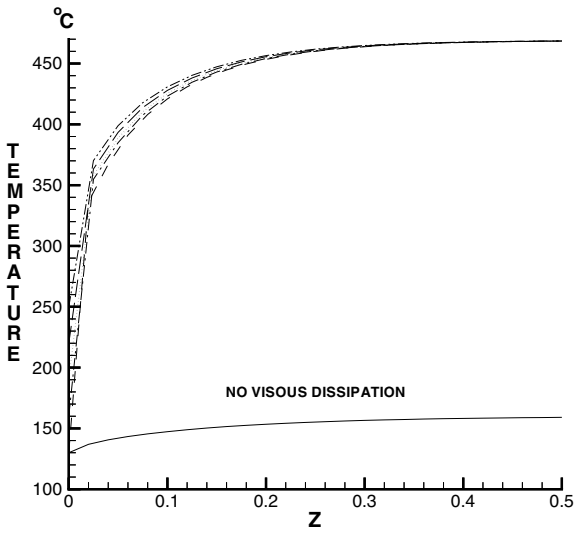

Fig. 5. Bulk temperature profiles as functions of dimensionless axial distance with various inlet temperatures: $T_0 = 130$ °C (dashed line), $T_0 = 190$ °C (dotted line), $T_0 = 220$ °C (long dashed line), $T_0 = 250$ °C (dash dotted line), $T_0 = 160$ °C (solid line) with no viscosity dissipation.

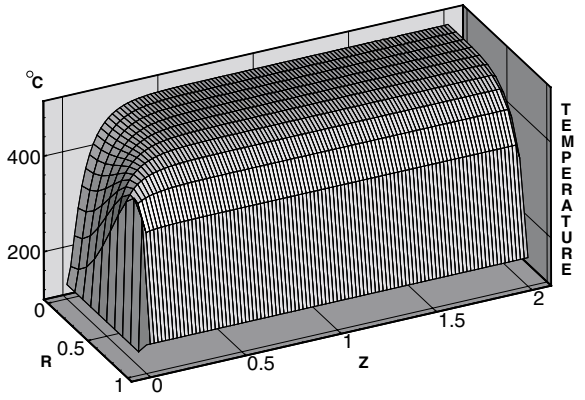

Fig. 6. Three dimensional temperature profile of the power-law flow in the tube.

different inlet temperatures. In each case of temperature-dependent models, the bulk temperature approaches the same outlet temperature, 462 °C. This is to be expected since the fully developed velocity and temperature profiles are determined by the wall boundary condition, the viscosity and thermal conductivity of the fluid, not by the inlet temperature of the fluid. It was pointed out by Faghri and Sparrow [5] that wall axial conduction can readily overwhelm fluid axial condition in a case for Newtonian flows. Also shown in Fig. 5 is the effect of removing the viscous dissipation term from the energy equation. Without viscous dissipation, the limiting bulk temperature is equal to the wall temperature of

160 °C. The difference of 302 °C is an indication of the importance of viscous dissipation in the Poiseuille flow of polymer melts through a tube. The temperature profile becomes fully developed after $Z = 0.2$, which is about 60 cm in the actual tube length. In Fig. 6, development of temperature profiles along two dimensions (R, Z) is presented.

Most of the previous contributions on forced heat transfer of power-law flows through a tube were for Newtonian fluid without considering viscous dissipation. Among them, Khellaf and Langiat [8] solved the Graetz problem in the entrance region of ducts. Wei and Zhang [17] found the steady state solution far away from the entrance for the same problem by using the Chambre method. Their solution can be expressed as

$$T = T_\infty - \frac{2C_1(v+2)}{nB(C_1+1)h} + \frac{2}{nB}\ln\frac{C_1R^{v+2}+1}{C_1+1}$$

for the problem with mixed boundary condition, where

$$C_1 = \sqrt{\left[\frac{CnB+(v+2)^2\,\mathrm{e}^{nBl}}{CnB}\right]^2 - 1} - \frac{CnB+(v+2)^2\,\mathrm{e}^{nBl}}{CnB}$$

$$C = \frac{u_{\mathrm{av}}^{n+1}}{k} A\,\mathrm{e}^{nBT_{\mathrm{m}}}\frac{(v+2)^{n+1}}{r_0^{n-1}}$$

and

$$l = T_\infty - \frac{2C_1(v+2)^2}{nB(C_1+1)h}$$

By letting $h \to \infty$ in the limiting case, the above solution becomes the solution of the corresponding problem with Dirichlet boundary condition, which is

$$T = T_{\mathrm{w}} + \frac{2}{nB}\ln\frac{C_1R^{v+2}+1}{C_1+1}$$

where

$$C_1 = \sqrt{\left[\frac{CnB+(v+2)^2\,\mathrm{e}^{nBT_{\mathrm{w}}}}{CnB}\right]^2 - 1} - \frac{CnB+(v+2)^2\,\mathrm{e}^{nBT_{\mathrm{w}}}}{CnB}$$

This is equivalent to applying the ambient temperature T_∞ directly to the fluid on the wall and letting $T_{\mathrm{w}} = T_\infty$. Fig. 7 presents a comparison at tube length approximately equals 60 cm between our finite element numerical solution and the corresponding analytic solution of Wei and Zhang with Dirichlet wall boundary condition. It can be seen that the agreement is good with a maximum deviation of 5.6%. This error is to be expected since the choice of the value of h, the finite element mesh and the round-off error in solving an $N \times N$ non-linear system with $N = 2000$ etc. are all contributing to this error. Since the standard Gauss–Jordon elimination and the backward substitution method are used to solve the linearized equation at each Newton's iteration, the round-off error in this linear algebraic solver does not seem to be the main reason for the discrepancies. Another analytical approach to the non-Newtonian fluids with viscous dissipation in circular tubes was presented by Flores et al. [4]. In their paper, they described a power-law fluid of constant thermophysical properties flowing in a laminar regime through a tube or a flat plate. Although their temperature-independent viscous dissipation term is different from our temperature-dependent viscous dissipation term, the algorithm needed to solve both problems is basically the same, except that we need to set the coefficient of the temperature-dependent part in our viscous dissipation term to zero. Therefore, by a small modification we solve their problem to test the reliability of our program. Their dimensionless energy balance equation is given as

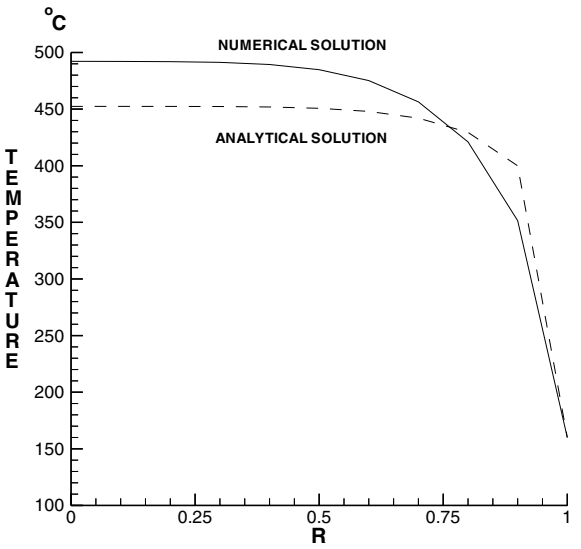

Fig. 7. Numerical solutions vs analytical solution at a large tube length of 60 cm.

$$(1-R^{n+1})\frac{\partial T}{\partial Z} = \frac{1}{R^M}\frac{\partial}{\partial R}\left(R^M\frac{\partial T}{\partial R}\right) + B_{\mathrm{r}}R^{n+1} \tag{4.1}$$

where the dimensionless transformation is given as

$$T = \frac{T-T_0}{T_{\mathrm{w}}-T_0}, \quad R = \frac{r}{r_0}$$

$$Z = n^*(M+1)\left(\frac{x}{R}\right)\frac{k}{\rho C_p u_{\mathrm{av}} R}$$

$$n^* = (M+1)^{-1} - (M+n+2)^{-1}$$

$$B_{\mathrm{r}} = \frac{b}{k(T_{\mathrm{w}}-T_0)}\left[u_{\mathrm{av}}(M+n+2)\right]^{\frac{n+1}{n}/R^{(1-n)/n}}$$

In the above, T is the dimensional temperature, r_0 is the radius of the tube or half thickness of a flat duct, r is the radial coordinate z is the axial flow coordinate, T_w and T_0 are the constant wall temperature and inlet temperature, respectively. The constant b is the shear rate viscosity, n the viscosity shear rate exponent ($n = 1$, Newtonian; $n > 1$, pseudoplastic behavior, and $n < 1$, dilatant behavior) and M is to denote the geometry. M is 0 when fluid is flowing on a plane, and M is 1 when fluid is flowing through a cylindrical tube. The Brinkman number, B_r, can be either positive or negative according to the value of $(T_w - T_0)$. Thus, $B_r < 0$ stands for cooled flow, while $B_r > 0$ when the flow is heated. Eq. (4.1) is similar to (2.8). So by a small modification, this problem can be solved by our program.

Fig. 8 presents a comparison of bulk temperature values generated by our program with those of Flores et al. The agreement is excellent, since the maximum deviation in the whole range of Z values is only about 0.4%. Both solutions seem to converge to the same value after $Z \geqslant 1$. In Fig. 9, the present numerical solution has a maximum deviation of 3.4% from the analytical solution of Flores et al. in the whole range of Z. In Fig. 10, the present numerical result has a maximum deviation of 5.1% from the analytical solution of Flores et al. in the whole range of Z. It can be concluded that the present numerical solution approximates the analytical solutions well for small values of D and for bulk temperatures. This justifies the reliability of the present numerical method and the finite element code. A grid refinement near the entrance is needed in order to compare the corresponding solutions for large values of D in more detail. However we do not intend to do such comparisons in this work.

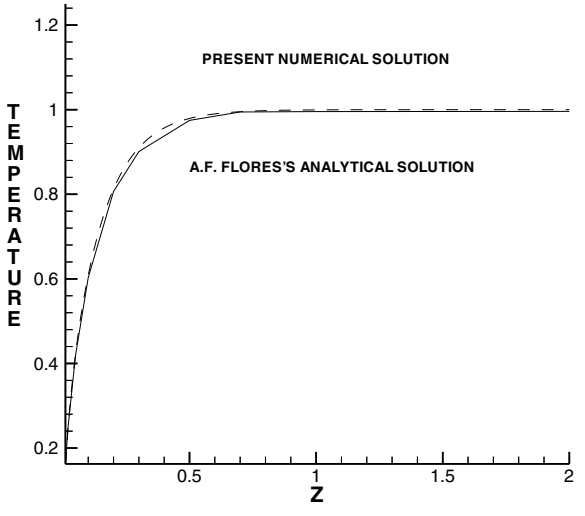

Fig. 8. Bulk temperature as a function of dimensionless axial distance: Present numerical solution vs the analytical solution of Flores et al. at $B_r = 0$.

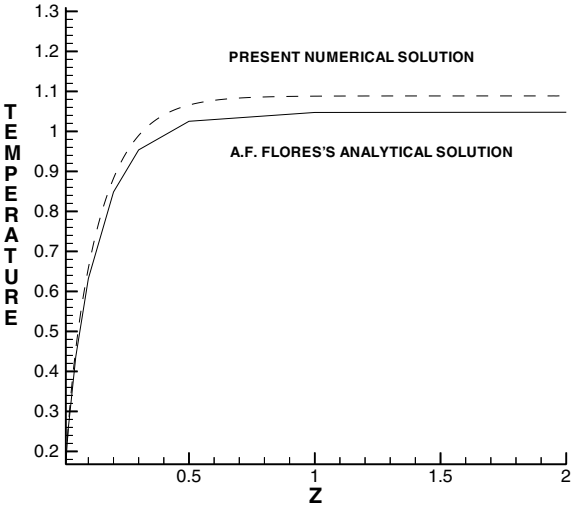

Fig. 9. Bulk temperature as a function of dimensionless axial distance: Present numerical solution vs the analytical solution Flores et al. at $B_r = 1$.

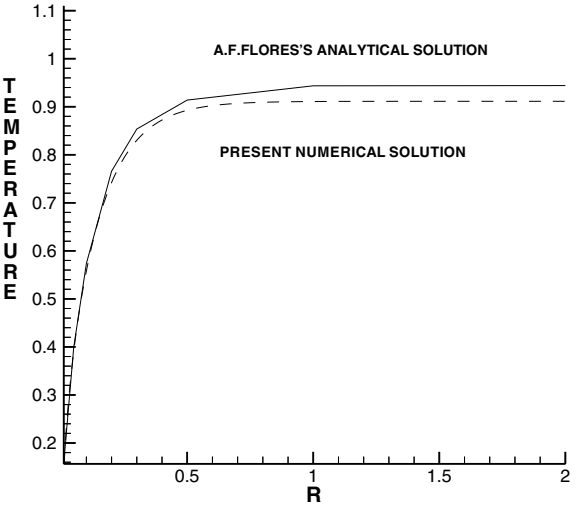

Fig. 10. Bulk temperature as a function of dimensionless axial distance: Present numerical solution vs the analytical solution of Flores et al. at $B_r = -1$.

5. Conclusion

A Graetz–Nusselt type problem of incompressible non-Newtonian fluids with temperature-dependent power-law viscous dissipation was investigated by using a Galerkin method with linear axisymmetric triangular

finite elements. The resulting system of non-linear algebraic equations was solved iteratively by using Newton's method. The result was validated by comparing the numerical steady state solution with the analytical steady state solution and tested by comparing the numerical solution with the analytical solution of a Graetz–Nusselt problem in a special case. It was shown that the temperature-dependent viscous dissipation term has significant impact on the heat transfer. Comparing with those models in which the conduction term in tube length direction was neglected, this model seems to represent the true solution better at the entrance region of the tube while imposing a zero longitudinal heat flux condition at large tube length. The bulk temperature difference between the model with temperature-dependent power-law viscous dissipation and the model without viscous dissipation is 302 °C for the given data. Further, the numerical results indicate that the temperature profile becomes fully developed at a tube length over $z = 60$ cm in the example. The finite element code developed can be used for similar problems with general boundary conditions and data in tubes. Finally, the results in this work are not applicable to fluids in which effective viscosity does not vanish near the centerline of the tube.

References

[1] E.E. Agur, J. Vlachopoulos, Heat transfer to molten polymer flow in tubes, J. Appl. Polym. Sci. 26 (1981) 765–773.

[2] R. Brewster, T. Irvine, Similitude considerations in laminar flow of modified power law fluids in circular ducts, Wärme- und Stoffübertragung 21 (1987) 83–86.

[3] J. Dunleavy, S. Middleman, Relation of shear behavier of solutions of polyisbutylene, Trans. Soc. Rheol. 10 (1966) 151–168.

[4] A.F. Flores, J.C. Gottifredi, G.V. Morales, O.D. Quiroga, Heat transfer to power-law fluids flowing in tubes and flat ducts with viscous heat generation, Chem. Engng. Sci. 46 (1991) 1385–1392.

[5] M. Faghri, E. Sparrow, Simultaneous wall and fluid axial conduction in laminar pipe-flow heat-transfer, ASME J. Heat Transfer 102 (1980) 58–63.

[6] P.N. Godbole, S. Nakazawa, O.C. Zienkiewicz, Blood flow analysis by the finite element method, in: International Conference on Finite Elements in Biomechanics, 1980, pp. 277–293.

[7] A. Kumar, M. Bhattacharya, Numerical analysis of aseptic processing of a non-Newtonian liquid food in a tubular heat exchanger, Chem. Engng. Commum. 103 (1991) 27–51.

[8] K. Khellaf, G. Lauriat, A new analytical solution for heat transfer in the entrance region of ducts: hydrodynamically developed flows of power-law fluids with constant wall temperature, Int. J. Heat Mass Transfer 40 (1996) 3443–3447.

[9] P. Lin, Y. Jaluria, Heat transfer and solification of polymer melt flow in a channel, Polym. Engng. Sci. 37 (1997) 1247–1258.

[10] W. Luelf, L. Burmeister, Viscous dissipation effect on pressure gradient for laminar flow of a non-Newtonian liquid through a duct of subfreezing wall temperature, ASME J. Heat Transfer 118 (1996) 973–977.

[11] B.C. Lychet, R.B. Bird, The Graetz–Nusselt problem for a power-law non-Newtonian fluid, Chem. Engng. Sci. 6 (1956) 35–41.

[12] R.L. Burden, J.D. Faires, Numerical Analysis, Academic Press, New York, 1997.

[13] J. Prusa, R.M. Manglik, Asymptotic and numerical solutions for thermally developing flows of Newtonian and non-Newtonian fluids in circular tubes with uniform wall temperature, Numer. Heat Transfer, Part A 26 (1994) 119–217.

[14] J.N. Reddy, Finite Element Method, McGraw-Hill, New York, 1993.

[15] L.J. Segerlind, Applied Finite Element Analysis, John Wiley, New York, 1984.

[16] V.P. Shih, C.C. Huang, S.Y. Tsay, Extended Leveque solution for laminar heat transfer to power-Law fluids in pipes with wall slip, Int. J. Heat Mass Transfer 38 (1995) 403–408.

[17] D. Wei, Z. Zhang, Decay estimates of heat transfer to molten polymer flow in pipes with viscous dissipation, Electron. J. Differen. Equat. 2001 (2001) 1–14.